A new dataset of river flood hazard maps for Europe and the Mediterranean Basin ~~region~~

Francesco Dottori[1], Lorenzo Alfieri[2], Alessandra Bianchi[3], Jon Skoien[1], Peter Salamon[1]

1: European Commission, Joint Research Centre, Via E. Fermi 2749, 21027 Ispra, Italy.

2: CIMA Research Foundation, Savona, Italy

3: FINCONS SPA, Italy

Correspondence to: francesco.dottori@ec.europa.eu

Keywords: river flooding, flood hazard mapping, Europe, EFAS, Mediterranean Basin ~~region~~.

Abstract

In recent years, the importance of continental-scale hazard maps for riverine floods has grown. Nowadays, such maps are used for a variety of research and commercial activities, such as evaluating present and future risk scenarios and adaptation strategies, as well as supporting national and local flood risk management plans. In this paper we present a new set of high-resolution (100 metres) hazard maps for river flooding that covers most European countries, as well as all of the river basins entering the Mediterranean and Black Seas in the Caucasus, Middle East and Northern Africa countries. The new river flood hazard maps represent inundation along 329,000 km of the river network, for six different flood return periods, expanding on the datasets previously available for the region. The input river flow data for the new maps are produced by means of the hydrological model LISFLOOD using new calibration and meteorological data, while inundation simulations are performed with the hydrodynamic model LISFLOOD-FP. In addition, we present here a detailed validation exercise using official hazard maps for Hungary, Italy, Norway, Spain and the UK, which provides a more detailed evaluation of the new dataset compared with previous works in the region. We find that the modelled maps can identify on average two-thirds of reference flood extent, but they also overestimate flood-prone areas for flood probabilities below 1-in-100 -years, while for return periods equal to or above 500 years

29 the maps can correctly identify more than half of flooded areas. Further verification is required

30 in North African and Eastern Mediterranean regions, in order to understand better the

31 performance of the flood maps in arid areas outside Europe. We attribute the observed skill to a

32 number of shortcomings of the modelling framework, such as the absence of flood protections

33 and rivers with upstream area below 500 km^2, and the limitations in representing river channels

34 and topography of low-land areas. In addition, the different designs of reference maps (e.g. extent

35 of areas included) affects the correct identification of the areas for the validation, thus penalizing

36 the scores. However, modelled maps achieve comparable results to existing large-scale flood

37 models when using similar parameters for the validation. We conclude that recently released high-

38 resolution elevation datasets, combined with reliable data of river channel geometry, may greatly

39 contribute to improving future versions of continental-scale river flood hazard maps. The new

40 high-resolution database of river flood hazard maps is available for download at

41 http://data.europa.eu/89h/1d128b6c-a4ee-4858-9e34-6210707f3c81 (Dottori et al., 2020a).

42

1) Introduction

Nowadays, flood hazard maps are a basic requirement of any flood risk management strategy (EC 2007). Such maps provide spatial information about a number of variables (e.g. flood extent, water depth, flow velocity) that are crucial to quantify flood impacts and therefore to evaluate flood risk. Moreover, they can be used as a powerful communication tool, enabling the quick visualization of the potential spatial impact of a river flood over an area.

In recent years, continental- and global-scale flood maps have grown in importance, and these maps are now used for a variety of research, humanitarian and commercial activities, and as a support of national and local flood management (Ward et al., 2015; Trigg et al., 2016). Global flood maps are used to provide flood risk information and to support decision-making in spatial and infrastructure planning, in countries where national level assessments are not available (Ward et al., 2015). Moreover, continental and global hazard maps are vital for consistent quantification of flood risk and for projecting the impacts of climate change (Alfieri et al., 2015; Trigg et al., 2016; Dottori et al., 2018), thereby allowing for comparisons between different regions, countries and river basins (Alfieri et al., 2016). Quantitative and comparable flood risk assessments are also necessary to derive measurable indicators of the targets set by international agreements such as the Sendai Framework for Disaster Risk Reduction (UNISDR, 2015).

In Europe, continental-scale flood hazard maps have been produced by Barredo et al. (2007), Feyen et al. (2012), Alfieri et al. (2014), Dottori et al. (2016a) and Paprotny et al. (2017). These maps have been used for a variety of studies, such as the evaluation of river flood risk under future socio-economic and climate scenarios (Barredo et al.,2007; Feyen et al., 2012; Alfieri et al., 2015), the evaluation of flood adaptation measures (Alfieri et al., 2016) and near-real-time rapid risk assessment (Dottori et al., 2017).

The quality of continental-scale flood maps is constantly improving, thanks to the increasing accuracy of datasets and modelling tools. Wing et al., (2017) developed a dataset of flood hazard maps for the conterminous United States using detailed national datasets and high-resolution hydrodynamic modelling, and demonstrated that continental-scale maps can achieve an accuracy similar to official national hazard maps, including maps based on accurate local-scale studies. Moreover, Wing et al. used the same official hazard maps to evaluate the performance of the global flood hazard model developed by Sampson et al. (2015). While the global model was less accurate than the continental version, it was able to identify correctly over two-thirds of flood

74 extent. Conversely, European-scale maps have undergone limited testing against official hazard

75 maps, due to limitations in accessing official data (Alfieri et al., 2014).

76 Here, we present a new set of flood hazard maps at 100 metres resolution (Dottori et al., 2020a),

77 developed as a component of the Copernicus European Flood Awareness System (EFAS,

78 www.efas.eu). The new dataset builds upon the map catalogue developed by Dottori et al (2016a),

79 and features several improvements. The geographical extent of the new maps has been expanded

80 to include all geographical Europe (with the exclusion of the Volga river basin), the rivers entering

81 the Mediterranean Sea and the Black Sea (with the partial inclusion of the Nile river basin), plus

82 Turkey, Syria and the Caucasus region. To the best of our knowledge, these are the first flood

83 hazard maps available at 100 metres resolution for the whole region of the Mediterranean Basin.

84 The hydrological input data are calculated using the latest version of the LISFLOOD hydrological

85 model (van der Knijff et al., 2010; Burek et al, 2013; https://ec-jrc.github.io/lisflood/), based on

86 updated routines and input data in respect to the previous dataset by Dottori et al. (2016a). Flood

87 simulations are performed with the hydrodynamic model LISFLOOD-FP (Bates et al., 2010;

88 Shaw et al., 2021), following the approach developed by Alfieri et al., (2014; 2015).

89 To provide a comprehensive overview of the skill of the new hazard maps, we perform a

90 validation exercise using official hazard maps for a number of countries, regions and large river

91 basins in Europe. The number and extent of the validation sites allows for a more detailed

92 evaluation with respect to previous efforts by Alfieri et al. (2014) and Paprotny et al. (2017), even

93 though none of the validation sites is located outside Europe (due the unavailability of national

94 flood maps). Finally, we discuss the results of the validation in light of previous literature studies,

95 we compare the performance of the present and previous versions of the flood hazard map dataset,

96 and we discuss a number of tests with alternative datasets and methods.

2) Data and methods

98 In this Section we describe the procedure adopted to produce and validate the flood hazard maps.

99 The hydrological input data consists of daily river flow for the years 1990-2016, produced with

100 the hydrological model LISFLOOD (see Section 2.1), based on interpolated daily meteorological

101 observations. River flow data are analysed to derive frequency distributions, peak discharges and

102 flood hydrographs, as described in Section 2.2. Flood hydrographs are then used to simulate

103 flooding processes at local scale with the LISFLOOD-FP hydrodynamic model (Section 2.3).

104   Finally, Section 2.4 describes the validation exercise and the comparison of different approaches
105   and input datasets.

2.1 The LISFLOOD model

107   LISFLOOD (Burek et al, 2013; van der Knijff et al., 2010) is a distributed, physically-based
108   rainfall-runoff model combined with a routing module for river channels. ~~In~~ For this work we
109   use~~d~~ an updated version of LISFLOOD, released as open-source software and available at
110   https://ec-jrc.github.io/lisflood/. The new version features an improved routine to calculate water
111   infiltration, the possibility of simulating open water evaporation and minor adjustments that
112   correct previous code inconsistencies (Arnal et al., 2019). The model is applied to run a long-term
113   hydrological simulation for the period 1990-2016 at 5 km grid spacing and at daily resolution,
114   which provides the hydrological input data for the flood simulations. Note that the same
115   simulation also provides initial conditions for daily flood forecast issued by EFAS.
116   The long-term run of LISFLOOD is driven by gridded meteorological maps, derived by
117   interpolating meteorological observations from stations and precipitation datasets (see Appendix
118   A for details). The meteorological dataset has been updated with respect to the dataset used by
119   Dottori et al. (2016a), to include new stations and gridded datasets across the new EFAS domain
120   (Arnal et al. 2019). In addition, LISFLOOD simulations require a number of static input maps
121   such as land cover, digital elevation model (DEM), drainage network, soil parameters and
122   parameterization of reservoirs. All the static maps have been updated to cover the whole EFAS
123   domain depicted in Figure 1. Further details on the static maps are provided by Arnal et al. (2019).
124   The current LISFLOOD version also benefits from an updated calibration at European scale,
125   based on the Evolutionary Algorithm approach (Hirpa et al., 2018) with the modified Kling-Gupta
126   efficiency criteria (KGE; Gupta et al., 2009) as objective function, and streamflow data for 1990-
127   2016 from more than 700 gauge stations. The same stations have been used to validate model
128   results, considering different periods of the time--series. The calibration and validation procedure
129   and the resulting hydrological skill are described ~~in~~ by Arnal et al (2019), and summarized in ~~the~~
130   Appendix B. While we did not carry out a formal comparison with the previous LISFLOOD
131   calibration, which used a different algorithm and performance indicators (Zajac et al., 2013), the
132   larger dataset of streamflow observations and the improvement of the calibration routines should
133   provide a better performance.

134   The geographical extent used in the present study to produce the flood maps follows the recent

135   enlargement of EFAS (Arnal et al., 2019), and is shown in Figure 1. The new domain is

136   approximately 8,930,000 km^2 wide (an increase of 76% compared with the previous extent). The

137   new extent covers the entire area of geographical Europe (with the exclusion of the Volga river

138   basin and a number of river basins of the Arctic Sea in Russia), all the rivers entering the

139   Mediterranean and Black Seas (with a partial inclusion of the Nile river basin), plus the entire

140   territories of Armenia, Georgia, Turkey, and most of Syria and Azerbaijan. The river network

141   included in the new flood hazard maps has a total length of 329,000 km, with an 80% increase

142   compared with the previous flood maps (Alfieri et al., 2015; Dottori et al., 2016a).

143

144   *Figure 1. Geographical extent of the EFAS extended domain covered by the present dataset of*

145   *flood hazard maps. The extent of the map dataset produced by Dottori et al. (2016a) is depicted*

146   *in beige, while the regions added with the extended domain are in green. The Figure also displays*

147   *the river network considered by the flood maps and the areas used for the validation exercise (see*

148   *Sections 2.3 and 3).*

2.2 Hydrological input of flood simulations

150   The hydrological input data required for the flood simulations are provided using synthetic flood

151   hydrographs, following the approach proposed by Alfieri et al. (2014).

152   We use the streamflow dataset derived from the long-term run of LISFLOOD described in Section

153   2.1, considering the rivers with upstream drainage areas larger than 500 km^2. This threshold was

154   selected because the meteorological input data cannot accurately capture the short and intense

155   rainfall storms that induce extreme floods in small river basins, and therefore the streamflow

156   dataset does not represent accurately the flood statistics of smaller catchments (Alfieri et al.,

157   2014).

158   For each pixel of the river network we selected annual maxima over the period 1990-2016 and

159   we used the L-moments approach to fit a Gumbel distribution and calculate peak flow values for

160   reference return periods of 10, 20, 50, 100, 200 and 500 years. We also calculated the 30- and

161   1,000-year return periods in limited parts of the model domain to allow validation against official

162   hazard maps, see Section 2.3. We used the Gumbel distribution to keep a parsimonious

163   parameterization (two parameters instead of three for the generalized extreme value (GEV), log-

164   normal and other distributions), thus avoiding over-parameterization when extracting high return

165   period maps from a relatively short time--series. The same distribution was also adopted for the

166   extreme value analysis in previous studies regarding flood frequency and hazard (Alfieri et al.,

167   2014, 2015; Dottori et al., 2016).

168   Subsequently, we calculate a Flow Duration Curve (FDC) from the streamflow dataset. The FDC

169   is obtained by sorting in decreasing order all the daily discharges, thus providing annual

170   maximum values Q_D for any duration i between 1 and 365 days. Annual maximum values are

171   then averaged over the entire period of data, and used to calculate the ratios ε_i between each

172   average maximum discharge for i--th duration $Q_{D(i)}$ and the average annual peak flow (i.e. $Q_D =$

173   1 day). Such a procedure was carried out for all the pixels of the river network.

174   The synthetic flood hydrographs are derived using daily time--steps. The peak value of the

175   hydrograph is given by the peak discharge for the selected T--year return period Q_T, while the

176   other values for Q_i are derived by multplying Q_T by the ratio ε_i. The hydrograph peak Q_T is placed

177   in the centre of the hydrograph, while the other values for Q_i are sorted alternatively to produce a

178   triangular hydrograph shape, as shown in Figure 2. The total duration of the synthetic hydrograph

179   is given by the local value of the time of concentration T_c, such that all of the durations $> T_c$ are

180   discarded from the final hydrograph (Figure 2).
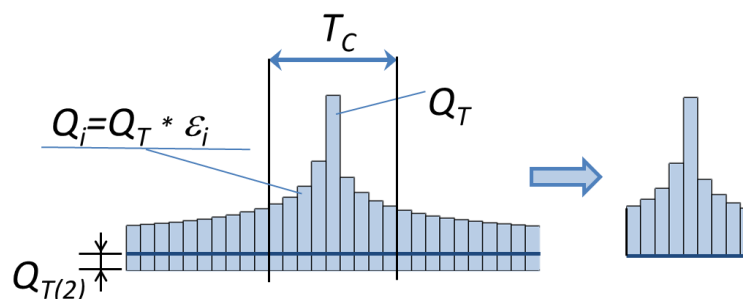
181

182   *Figure 2. General scheme of flood hydrographs (adapted from Alfieri et al., 2014).*

183

184   Because river channels are usually not represented in continental-–scale topography, flood

185   hydrograph values are reduced by subtracting the 2-years discharge peak $Q_{T(2)}$, which is

186   commonly considered representative of river bank-full conditions. (Note that the original DEM

187   is not modified with this procedure). Hence, the overall volume of the flood hydrograph is given

188   by the sum of all daily flow values with duration $< T_c$.

189

2.3 Flood hazard mapping

191   The continental-scale flood hazard maps are derived from local flood simulations run along the

192   entire river network, as in Alfieri et al. (2014). We use the DEM at 100 metres resolution

193   developed for the Catchment Characterization and Modelling Database (CCM; Vogt et al., 2007)

194   to derive a high-resolution river network at the same resolution. Along this river network we

195   identify reference sections every 5 km along stream-wise direction, and we link each section to

196   the closest upstream section (pixel) of the EFAS 5 km river network, using an partially automated

197   procedure to ensure a correct linkage near confluences. In this way, the hydrological variables

198   necessary to build the flood hydrographs can be transferred from the 5 km to the 100 metres river

199   network. Figure 3 describes how the 5 km and 100 metres river sections are linked using a

200   conceptual scheme.

Then, for every 100 metres river section we run flood simulations using the two-dimensional hydrodynamic model LISFLOOD-FP (Shaw et al., 2021), to produce a local flood map for each of the six reference return periods. Simulations are based on the local inertia solver of LISFLOOD-FP developed by Bates et al. (2010), which is now available as open-source software (https://www.seamlesswave.com/LISFLOOD8.0). We use the CCM DEM as elevation data, the synthetic hydrographs described in Section 2.2 as hydrological input data, and a mosaic of CORINE Land Cover for the year 2016 (Copernicus LMS, 2017) and Copernicus GlobCover (Global Land Cover Map) for the year 2009 (Bontemps et al., 2009) to estimate the friction coefficient based on land use.

Finally, the flood maps with the same return period are merged together to obtain the continental-scale flood hazard maps. The 100 metres river network is included as a separate map in the dataset, to delineate those water courses that were considered in the creating the flood hazard maps.
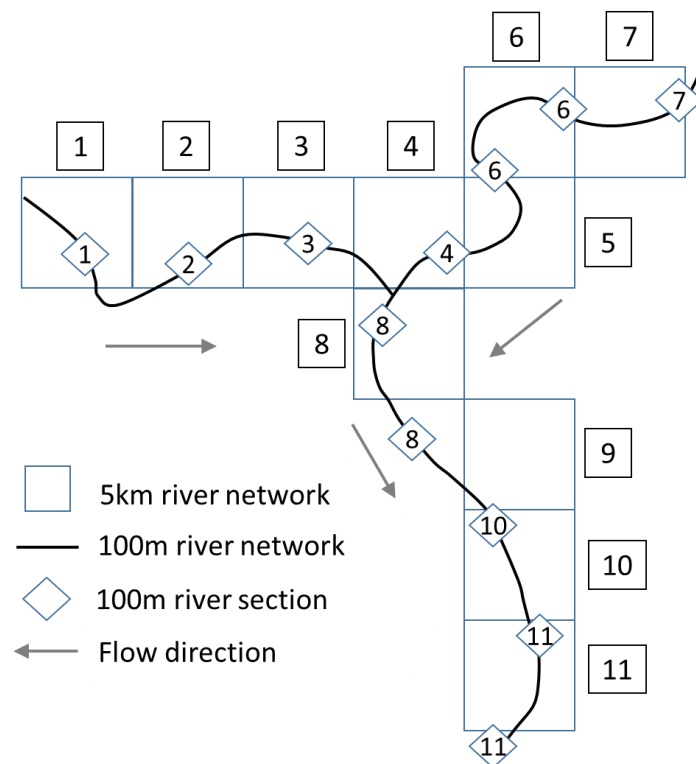
Figure 3. Conceptual scheme of the EFAS river network (5 km, squares) with the high-resolution network (100 metres) and river sections (diamonds) where flood simulations are derived. The related sections of the two networks are indicated by the same number. Source: Dottori et al. (2017).

219   It is important to note that the flood maps developed do not account for the influence of local

220   flood defences, in particular dyke systems. Such limitation has been dictated mainly by the

221   absence of consistent data at European scale. None of the available DEMs for Europe have has

222   the required accuracy and resolution to embed artificial embankments into elevation data.

223   Furthermore, there are no publicly available continental or national datasets describing the

224   location and characteristics (e.g. dyke height, distance from river channel) for flood protections.

225   Currently available datasets are based on the design return period of flood protection, e.g. the

226   maximum return period of flood events that protections can withstand before being overrun,

227   (Jongman et al., 2014; Scussolini et al., 2016). Most of the protection standards reported by these

228   datasets for Europe are based on empirical regressions derived using proxy variables (e.g. GDP,

229   land use), with few data based on actual design standards. While these datasets have been applied

230   to calculate flood risk scenarios (Alfieri et al., 2015) and flood impacts (Dottori et al., 2017), they

231   have important limitations when used for mapping flood extent. Wing et al. (2017) linked the

232   flood return period of protection standards with flood frequency analysis to adjust the bank height

233   of the river channels, however with impaired performance of the model. Moreover, recent studies

234   for United States suggest that empirical regressions based on gross domestic product and land use

235   may not be reliable (Wing et al., 2019).

236   Despite these limitations, maps not accounting for physical flood defences may be applied to

237   estimate the flood hazard in case of failure of the protection structures, and for flood events

238   exceeding protections levels.

2.3 Validation of flood hazard maps

2.3.1 Selection of validation areas and maps

241   The validation of large-scale flood hazard maps requires the use of benchmarks with one or more

242   datasets with extension and accuracy commensurate to the modelled maps. For instance Wing et

243   al. (2017) used the official hazard maps developed for the conterminous United States to evaluate

244   the performance of two flood hazard models, respectively designed to produce global-scale and

245   continental-scale flood maps (see Section 1). In Europe, all EU Member States as well as the UK

246   have developed national datasets of flood hazard maps for a range of flood probabilities (usually

247   expressed with the flood return period), following the guidelines of the EU Floods Directive (EC

248 2007). These maps are usually derived using multiple hydrodynamic models of varying
249 complexity (AdB Po, 2012) based on high-resolution topographic and hydrological datasets, such
250 as DEMs of at least 5 metres resolution in England (Sampson et al., 2015), LIDAR elevation data
251 in Spain (MITECO 2011), and river sections based on LIDAR surveys in the Po River basin (AdB
252 Po, 2012). Although official maps might be either prone to errors or incomplete (Wing et al
253 2017), these are likely to provide a higher accuracy than the modelled maps presented here, and
254 therefore they have been selected as reference maps for the validation. While official flood maps
255 are generally available online for consultation on Web-GIS services, only few countries and river
256 basin authorities make the maps available for download in a format that allows comparison with
257 geospatial data. Table 1 presents the list of flood hazard maps that could be retrieved and used for
258 the validation exercise, while their geographical distribution is shown in Figure 1. Note that the
259 relevant links to access these maps are provided in the Data Availability section.

260 While more of such official maps are likely to become available in the near future, the maps here
261 considered here offer an acceptable overview of the different climatic zones and floodplain
262 characteristics of the European continent. Conversely, we could not retrieve national or regional
263 flood hazard maps outside Europe, meaning the skill of the modelled maps could not be tested in
264 the arid regions in Northern Africa and Eastern Mediterranean. In Norway, Spain, the UK and the
265 Po River Basin the official maps take flood defences into account, which are not represented in
266 the modelling framework. Official maps for England also include areas prone to coastal flooding
267 events (such as tidal and storm surges). None of the official maps include areas prone to pluvial
268 flooding, which are therefore not considered in this analysis.

269 As mentioned in Section 2.3, the modelled maps do not include the effect of flood protections.
270 Wherever possible, for the comparison exercise we selected either reference flood maps that do
271 not account for protections (e.g. Hungary) or maps for flood return periods exceeding local
272 protection standards, assuming that the resulting flood extent is relatively unaffected by flood
273 defences. For example, the main stem of the Po river is protected against 1-in-200-year flood
274 events (Wing et al., 2019), whereas protection standards in England and Norway are usually
275 above 20 years (Scussolini et al., 2016). Reference maps where the extent and design level of
276 protection are not known (e.g. Spain) have been also included in the comparison to increase the
277 number of validation areas.

278

Country	Geographical extent	Return periods used	Defences included
Hungary	Country scale	30 - 100 – 1,000 years	No
Italy	Po River Basin	500 years	Yes
Norway	Country scale	100 years	Yes
Spain	Country scale	10 - 100 - 500 years	Yes
UK	England	100 – 1,000 years	Yes

279 *Table 1. Characteristics of the flood hazard maps used in the validation exercise. The links for*
280 *downloading the maps are provided in the Data Availability section.*

2.3.2 Performance metrics and validation procedure

282 The national flood hazard maps listed in Table 1 are provided as polygons of flood extent, with
283 no information on water depth or on original resolution of data. According to Sampson et al.
284 (2015), the official flood hazard maps for England are constructed using DEMs of at least 5 metres
285 resolution, therefore flood extent maps should be of comparable resolution. Reference flood maps
286 for the Po basin and Spain are likely to have a similar resolution since they are based on LIDAR
287 elevation data (AdB Po, 2012; MITECO 2011). For the comparison, official reference maps have
288 been converted to raster format with the same resolution as the modelled maps (i.e. 100 metres),
289 while the latter have been converted to binary flood extent maps. To improve the comparison
290 between modelled and reference maps we applied a number of corrections. Firstly, we used the
291 CORINE Land Cover map to exclude permanent water bodies (river beds of large rivers or
292 estuaries, lakes, reservoirs, coastal lagoons) from the comparison. Secondly, we restricted the
293 comparison area around modelled maps to exclude the elements of river network (e.g. minor
294 tributaries) included in the reference maps but not in the modelled maps. We used a different
295 buffer extent according to each study area, considering the floodplain morphology and the
296 variable extent and density of mapped river network. For example, in Hungary we applied a 10-
297 km buffer around modelled maps to include the large flooded areas reported in reference maps
298 and to avoid overfitting. In England, we used a 5 km buffer due to the high density of the river

network mapped in the official maps. The buffer is also applied to mask out coastal areas far from rivers estuaries, because official maps include flood-prone areas due to 1-in-200-year coastal flood events. We calculated that flood-prone areas inside the 5 km buffer correspond to 73% of the total extent for the 1-in-100-year flood. For the Po river basin, we excluded from the comparison the areas belonging to the Adige river basin and the lowland drainage network, which are not included in the official hazard maps. In Spain and Norway official flood hazard maps have only been produced where relevant assets are at risk, according to available documentation [MITECO 2011; NVE 2020]. We therefore restricted the comparison only to areas where official flood hazard maps have been produced. Table 2 provide the list of parameters used to determine the areas used for the comparison.

Test area	Buffer value (reference maps)	Buffer value (modelled maps)
Hungary	NA	10 km
Po River Basin	NA	See main text
Norway	5 km	5 km
Spain	5 km	5 km
England	NA	5 km

Table 2. List of parameters used to determine the extent of areas used for comparing reference and modelled maps (NA: buffer not applied).

We evaluate the performance of simulated flood maps against reference maps using a number of indices proposed in literature (Bates and De Roo, 2000; Alfieri et al., 2014; Dottori et al., 2016b; Wing et al., 2017). The hit ratio (HR) evaluates the agreement of simulated maps with observations and it is defined as:

$$HR = (Fm \cap Fo)/(Fo) \times 100 \qquad (1)$$

where $Fm \cap Fo$ is the area correctly predicted as flooded by the model, and Fo indicates the total observed flooded area. HR scores range from 0 to 1, with a score of 1 indicating that all wet cells

319   in the benchmark data are wet in the model data. The formulation of the HR does not penalize

320   over-prediction, which can be instead quantified using the false alarm ratio FAR:

321                 $FAR = (Fm/Fo)/(Fm) \times 100$ (2)

322   where Fm/Fo is the area wrongly predicted as flooded by the model. FAR scores range from 0

323   (no false alarms) to 1 (all false alarms). Finally, a more comprehensive measure of the agreement

324   between simulations and observations is given by the critical success index (CSI), defined as:

325                 $CSI = (Fm \cap Fo)/(Fm \cup Fo) \times 100$ (3)

326   where $Fm \cup Fo$ is the union of observed and simulated flooded areas. CSI scores range from 0

327   (no match between model and benchmark) to 1 (perfect match between benchmark and model).

2.4 Additional tests

329   To choose the best possible methodologies and datasets to construct the flood hazard maps, we

330   performed a number of tests using recent input datasets, as well as alternative strategies to account

331   for vegetation effects on elevation data.

2.4.1 Elevation data

333   It is well recognized that the quality of flood hazard maps strongly depend on the accuracy of

334   elevation data used for modelling (Yamazaki et al., 2017). This is especially crucial for

335   continental-scale maps, since the quality of available elevation datasets is rarely commensurate

336   to the accuracy required for modelling flood processes [Wing et al., 2017]. Moreover, high-

337   resolution and accurate elevation data such as LIDAR-based DEMs cannot be used for reasons of

338   consistency, since these data are only available for few areas and countries.

339   The recent release of new global elevation models have the potential to improve the accuracy of

340   large-scale flood simulations, and hence the quality of flood hazard maps. Here, we test the use

341   of the MERIT DEM (Yamazaki et al., 2017) within the proposed modelling approach and we

342   compare the results with those obtained with CCM DEM. The MERIT DEM is based on the

343   SRTM data, similarly to CCM DEM, but has been extensively corrected and improved through

344   comparisons with other large-scale datasets, to eliminate error biases, improve data accuracy at

345   high latitudes (areas above 60° are not covered by SRTM), and compensate for factors like

346   vegetation cover. Note that areas above 60° in CCM DEM were derived from national datasets,

347   and therefore these areas are where the two datasets are likely to differ most.

2.4.2 Correction of elevation data with land use

The CCM DEM elevation dataset is mostly based on SRTM data, and so the elevation values can be spuriously increased by the effect of vegetation canopy in densely vegetated areas, and by buildings in urban areas. Recent research work has proposed advanced techniques to remove surface artefacts, based on artificial neural networks (Wendi et al., 2016, Kulp and Strauss, 2018) or other machine learning methods (Liu et al., 2018; Meadows and Wilson, 2021). Most approaches correct DEM elevation with higher-accuracy datasets, using auxiliary data such as tree density and height for correcting vegetation bias (as done for the MERIT-DEM by Yamazaki et al., 2017), whereas elevation bias in urban areas can be corrected using night light, population density, or Open-Street-Map elevation data (Liu et al., 2018). Given that improving elevation data is not the main scope of this work, we opted for applying a simpler method for quickly correcting the CCM DEM elevation data. Specifically, we use the land cover map derived from CORINE Land Cover and Copernicus GlobCover to identify densely vegetated areas and urban areas, and we applied a correction factor as a function of local land use to reduce elevation locally. The correction factor varies from 8 metres for dense forested areas, to 2 metres for urban areas. Note that these values are based on the findings of previous literature studies such as Baugh et al. (2013) and Dottori et al. (2016b), while a formal calibration was not undertaken.

3) Results and discussion

We present the outcomes of the validation exercise by first describing the general results at country and regional scale (Section 3.1). Then, we discuss the outcomes for England, Hungary and Spain (Section 3.2), while the Norway and Po river basin case studies are presented in the Appendix C. We also complement the analysis with additional validation over major river basins in England and Spain. In Section 3.3 we compare our results with the validation exercise carried out by Wing et al. (2017) and with the findings of other literature studies. Finally, in Section 3.4 and 3.5 (and Appendix B) we compare the performance of the present and previous versions of the flood hazard map dataset, and we discuss the results of the tests with different elevation data and strategies to account for vegetation.

3.1 Validation of modelled maps at national and regional scale

Table 3 presents the results of the validation for each testing area and return period. The performance metrics are calculated using the total extent of the reference and modelled maps with the same return period. The first visible outcome is the low scores for the comparisons with reference maps with high probability of flooding, i.e. low flood return periods (<_30 years). Performances improve markedly with the increasing of return periods due to the decrease of false alarm rate (FAR), while the hit rate (HR) does not vary significantly. In particular, critical success index (CSI) values approach 0.5 for the low probability flood maps, i.e., for return periods equal or above 500 years. Considering that most of the reference flood maps include the effect of flood defences (unlike the modelled maps), these results suggest that the majority of rivers in the study areas may be protected for flood return periods of around 100 years or less, as indeed reported by available flood defence databases (Scussolini et al., 2016). Differences between simulated and reference hydrological input are likely to influence the skill of modelled flood maps and may depend on several factors such as the hydrological model performance for peak flows, extreme value analysis (distribution used for extreme value fitting, length of available time-series) design hydrograph estimation. However, further analysis is difficult as we have no specific information on the hydrological input used for the reference flood maps (e.g. peak flows, statistical modelling of extremes, hydrograph shape). In the following Sections, we use the skill of the LISFLOOD long-term simulation to evaluate the agreement between modelled and observed hydrological regime, but this does not necessarily translate to extreme values. High-probability floods are also sensitive to the method used to reproduce river channels, and the simplified approach used in this study might underestimate the conveyance capacity of channels (see Section 3.2.2 for an example). Finally, the better performance for low-probability floods may also depend on floodplain morphology, where valley sides create a morphological limit to flood extent.

Table 3. Results of the validation against official flood hazard maps: value of the performance indices at country and regional scale. RP=Return Period, HR=Hit Ratio, FAR= False Alarm Ratio, CSI=Critical Success Index.

REGION	RP (years)	HR	FAR	CSI
Spain	10	0.58	0.65	0.28
Hungary	30	0.77	0.88	0.11
Spain	100	0.63	0.44	0.42
Hungary	100	0.76	0.74	0.24
Norway	100	0.70	0.72	0.25
England	100	0.53	0.31	0.43
Po River Basin	500	0.60	0.13	0.56
Spain	500	0.61	0.36	0.45
Hungary	1000	0.76	0.45	0.47
England	1000	0.52	0.12	0.48

3.2 Discussion of results at national and regional scale

The results in Table 3 highlight considerable differences in the skill of the flood maps across countries and regions. While some differences may arise from the variability of floodplain morphology and model input data, others are attributable to the different methods applied to produce the reference maps (MITECO 2011; NVE 2020). In the following sections we examine in more detail the outcomes for each study area.

3.2.1 England

According to Table 3, modelled flood maps tend to underestimate flood extent in England, as visible by the HR values around 0.5 (e.g. out of every two flooded cells, only one is correctly identified as flooded by the model). Such result is confirmed when focusing the analysis on the major river basins of England, as reported in Table 4. Notably, HR has generally marginal or no increases with the increase of return period considered, while FAR values have a marked decrease. The results of reported by Arnal et al. (2019) and summarized in Figure B1 suggest a

423 fair hydrological skill of the LISFLOOD calibration in England, with KGE values generally above
424 0.5. However, there is not a clear correlation between hydrological and flood map skill, with some
425 basins (e.g. Thames) showing high KGE values but relatively low CSI values.
426 For the Thames basin, the low CSI value is likely influenced by the tidal flooding component
427 from London eastwards. According to Sampson et al. (2015), the official flood hazard map
428 assumes a 1 in 200 year coastal flood along with failure of the Thames tidal barrier, whereas our
429 river flood simulations use the mean sea level as boundary condition and do include storm surge
430 and tidal flooding. Concurrent fluvial-tidal flooding processes occur in other river estuaries, so
431 this might reduce the skill of the modelled maps. Furthermore, the Thames catchment is heavily
432 urbanized and has extensive flood defencse and alleviation schemes compared the other
433 catchments (Sampson et al., 2015). Both aspects might increase the elevation bias of CCM DEM
434 and complicate the correct simulation of extreme flood events.

435 *Table 4. Validation indices in England and in major river basins.*

436

Catchments	100-year RP			1,000-year RP		
	HR	**FAR**	**CSI**	**HR**	**FAR**	**CSI**
England	**0.53**	**0.31**	**0.43**	**0.52**	**0.12**	**0.48**
Ouse	0.57	0.39	0.42	0.56	0.19	0.49
Severn	0.64	0.24	0.53	0.63	0.20	0.54
Thames, above Lea	0.56	0.46	0.38	0.55	0.23	0.47
Trent	0.63	0.28	0.50	0.59	0.06	0.57
Tyne	0.51	0.43	0.37	0.52	0.28	0.43

437
438
439 Besides these results, the visual inspection of reference maps suggest that the underestimation is
440 partly caused by the high density of mapped river network in the reference maps, in respect to
441 modelled maps. Indeed, the modelling framework excludes river basins with an upstream basin
442 area below 500 km^2, meaning that EFAS maps only cover main river stems but miss out several
443 smaller tributaries. This is clearly visible over the Severn and in the upper Thames basins (Figure
444 4), and might also explain the lower skill in the lowlands of Ouse and Trent rivers, where the
445 contributions of main river stems and tributaries to the flood extent are difficult to separate.

446   Including minor tributaries in the flood maps would require either to increase the resolution of

447   the climatological forcing to reproduce intense local rainfall, or to add a pluvial flooding

448   component as done by Wing et al. (2017). Finally, areas prone to storm surge and tidal flooding

449   around river estuaries might further reduce the overall skill of modelled maps, despite the 5 km

450   buffer applied.
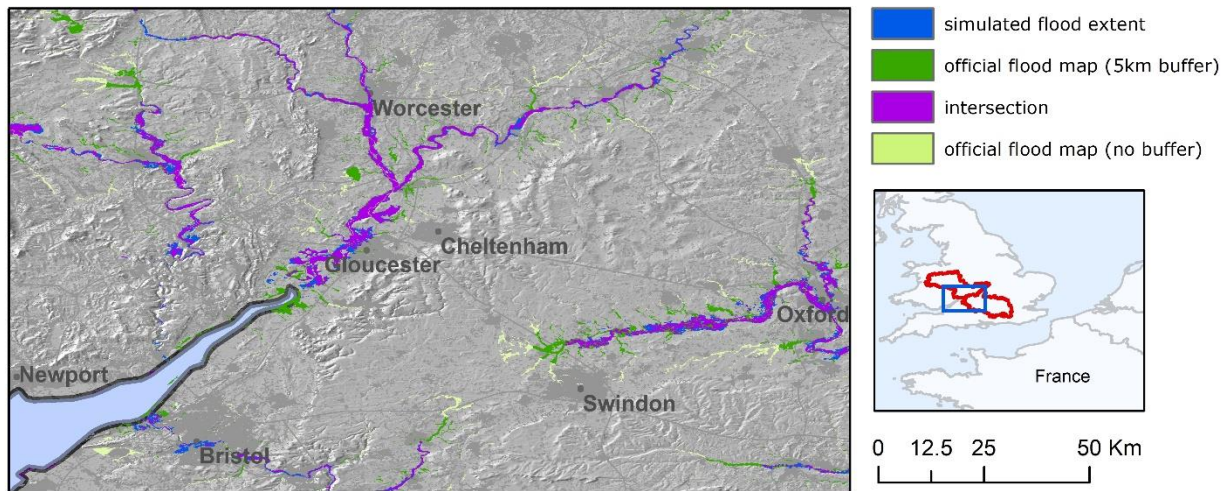
451

452   *Figure 4. Comparison of modelled (blue) and reference (green) flood hazard maps (1-in-100-*

453   *year) over the Severn (centre) and the upper Thames (right) river basins in England. Purple*

454   *areas denotes intersection (agreement) between the modelled and reference set of maps. The*

455   *original reference maps (i.e. with no masking around modelled maps) are shown in light green.*

456

3.2.2 Hungary

458   The results in Table 3 for Hungary show a general tendency to overestimate flood extent for all

459   return periods. HR values are consistently high and do not change much with the return period.

460   Conversely, FAR is very high for the 1-in-30 year flood map and still considerable even for the

461   1-in-1000 year flood map. Arnal et al (2019) reported a fair hydrological skill of LISFLOOD

462   (KGE values >0.5) for the calibration period, even though KGE validation values were

463   considerably low for the Tisza River.

464   Given that flood defences are not modelled in reference maps, the observed results may be

465   explained by assuming a large conveyance capacity of river channels. For instance, the 1-in-100

466   year reference map show relatively few flooded areas for the Danube main stem (Figure 5), thus

467 suggesting that the main channels can convey the 1-in-100-year discharge without overflowing.
468 Conversely, river channels in the modelling framework are assumed to convey only the 1-in-2-
469 year discharge. Obviously, the same considerations can be made for 1-in-30-year discharge for
470 the majority of river network, which explains the very low scores. Furthermore, artificial
471 structures such as road embankments and drainage network may further reduce flood extent in
472 lowland areas, leading to further overestimation given the fact that these features are not
473 represented in the DEM. These findings highlight the need for high-resolution DEM fed with
474 local-scale information to achieve adequate performance in lowland areas, as observed also by
475 Wing et al (2019b).
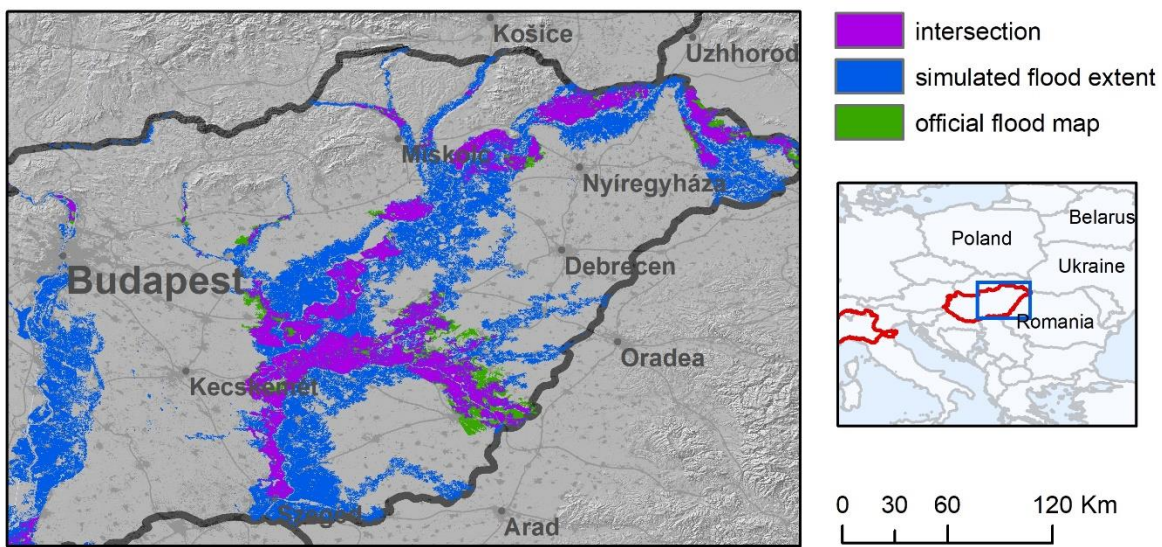
476

477 *Figure 5. Comparison of modelled (blue) and reference (green) flood hazard maps (1-in-100-*
478 *year) over the Danube (left) and Tisza (right) rivers in Hungary. Purple areas denotes the*
479 *intersection between the modelled and reference set of maps.*

480

3.2.3 Spain

482 The performance of the modelled maps in Spain show a fairly stable HR value and decreasing
483 FAR values with increasing return periods, similarly to what was observed for England and
484 Hungary. The analysis of the results for the major river basins of the Iberian Peninsula, reported
485 in Table 5, provide further insight on the skill of flood maps. A number of basins exhibit both
486 large HR and FAR such as the Duero, Tajo and Guadalquivir basins. Rivers in South-East Spain
487 (Segura, Jucar) have relatively low HR values, while the modelled maps perform better in the

Ebro river basin. The interpretation of results requires the consideration of different aspects. The poor results for the 1-in-10-year maps are likely due to the effect of flood protection structures, such as dykes and flood regulation systems, which are probably relevant also for the 1-in-100-year map. Indeed, most Iberian rivers are regulated by multiple reservoirs, which are often used to reduce flood peaks according to specific operating rules. While dykes are not represented in the inundation model, reservoirs are included in the LISFLOOD model through a simplified approach, given that operating rules are not known. Therefore, the real and modelled hydrological regimes might differ significantly, including flow peaks of low-probability flood events. This is reflected also by the low hydrological skill of LISFLOOD, with KGE values generally below 0.5 with few exceptions (Figure B1).

In addition, the comparison of modelled and reference maps is affected by the partial coverage of the reference inundation maps in several river basins. According to the information available in the official website (MITECO 2011) large sections of the river network in the basins of the Duero, Tajo, Guadiana and Guadalquivir rivers have not been analysed, due to the absence of relevant assets or inhabited places at risk. Even though this has been accounted by restricting the area of comparison around reference maps, a visual inspection of the maps being compared shows spurious overestimation around the edges of reference map polygons (Figure 6). Finally, the low HR values scored in rivers in South-East Spain (Segura, Jucar) are partially explained by the presence of several tributaries not included in EFAS maps.

Table 5. Validation indices in Spain and in some test river basins.

Catchments	10-year RP			100-year RP			500-year RP		
	HR	**FAR**	**CSI**	**HR**	**FAR**	**CSI**	**HR**	**FAR**	**CSI**
Spain	**0.58**	**0.65**	**0.28**	**0.63**	**0.44**	**0.42**	**0.61**	**0.36**	**0.45**
Duero	0.60	0.74	0.22	0.65	0.55	0.36	0.65	0.46	0.42
Ebro	0.71	0.46	0.45	0.75	0.27	0.59	0.74	0.23	0.61
Guadalquivir	0.67	0.66	0.29	0.69	0.49	0.42	0.66	0.46	0.42
Guadiana	0.52	0.63	0.28	0.60	0.42	0.42	0.61	0.31	0.48
Jucar	0.32	0.89	0.09	0.53	0.46	0.36	0.51	0.39	0.39
Tajo	0.60	0.85	0.14	0.70	0.63	0.32	0.69	0.49	0.41
Segura	0.18	0.89	0.07	0.38	0.52	0.27	0.41	0.24	0.36

509
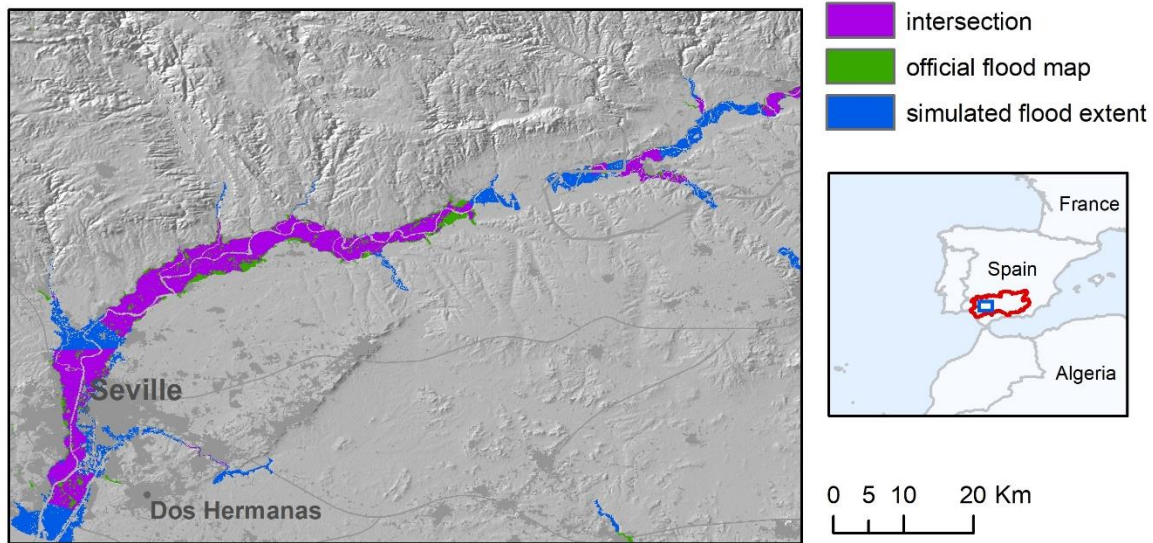
Figure 6. Comparison of modelled (blue) and reference (green) flood hazard maps (1-in-100-year) over a stretch of the Guadalquivir river basin, Spain. Purple areas denote the intersection between the two set of maps.

3.3 Comparison with previous continental-scale validation studies

To put the previously described results in context, we compare them with the validation exercises performed by Sampson et al. (2015) over the Thames and Severn rivers in England, and by Wing et al. (2017) over United States. The study by Wing et al. is, to our knowledge, the first study that carried out a consistent validation of modelled flood hazard maps at continental scale. Bates et al. (2021) have recently updated the work by Wing et al. by including pluvial and coastal flooding components in the modelling framework, but their work is not considered here. A comparison of validation metrics of the three studies are shown in Table 6 and 7. For our framework, we calculated each index in Table 6 using the overall modelled and reference flood extent available for each return period (e.g. the value for the 100-year maps includes reference and modelled maps for England, Spain and Norway). As such, each area is weighted according to the extent of the corresponding flood map.

As can be seen in Table 6, the continental-scale model by Wing et al. achieved the highest scores both for 100-year and 500-year return periods. However, this model is based on national datasets with higher accuracy and resolution than those available for the European continent (e.g. a 10 metres resolution DEM and a detailed catalogue of flood defences). The global and European

529 models have comparable hit rates for the 100-year flood maps (0.68 and 0.65 respectively), but

530 the former exhibits a much lower FAR value (0.34 compared to 0.61 for the European model),

531 and a higher HR value for the 500-year maps.

532 The higher HR values scored by the US and global models might depend on the higher density of

533 the modelled river network, which includes river reaches up to 50 km^2 by simulating both pluvial

534 and fluvial flooding processes. The lower FAR values of the US and global models might be

535 explained by the inclusion of flood defences. In the US model, defences are explicitly modelled

536 using the US dataset of flood defences, while the global model parameterizes flood defences

537 through the adjustment of channel conveyance using socioeconomic factors and degree of

538 urbanization (Wing et al., 2017). However, Wing et al observed that the latter methodology had

539 a negligible effect on HR values in defended areas, when compared with an undefended version

540 of the model.

541 Another possible reason for the low FAR values is the different approach used in the validation

542 method. Wing et al. applied a narrow 1 km buffer around official maps to constrain the area of

543 comparison and avoid spurious over-prediction in areas not considered by official maps.

544 However, this might result in a reduction of true false alarms, because part of overestimated flood

545 areas can go undetected. To verify this hypothesis, we recalculated the performance indices

546 against the 100-year reference map in Spain using a 1 km buffer instead of the 5 km previously

547 applied to constrain the validation area. As a result the FAR dropped from 0.44 to 0.34, similar

548 to the performance of the global model. However, we observed- a reduction of true false alarms,

549 especially in river basins with continuous map coverage such as the Ebro, Jucar and Segura.

550 *Table 6. Comparison of the performance metrics for the European model described in the present*

551 *study and the two models evaluated in the study by Wing et al. (2017).* ——

	RP (years)	HR	FAR	CSI
US model (Wing et al.)	100	0.82	0.37	0.55
Global model (Wing et al.)	100	0.69	0.34	0.50
European model (this study)	100	0.66	0.61	0.32
US model (Wing et al.)	500	0.86	na	na
Global model (Wing et al.)	500	0.74	na	na
European model (this study)	500	0.61	0.24	0.51
European model (this study)	1000	0.68	0.39	0.47

552

553   The comparison of HR, FAR and CSI values show better scores for the global maps by Sampson

554   et al. (2015) in respect to our modelled maps (Table 7).

555

556   *Table 7. Comparison of the performance metrics for the maps described in the present study and*

557   *the global maps by Sampson et al. (2015). Metrics for the latter study are calculated removing*

558   *all channels with upstream areas of less than 500 km2.*

	HR	**FAR**	**CSI**
Thames (this study)	0.56	0.46	0.38
Thames (Sampson et al. 2015)	0.73	0.3	0.56
Severn (this study)	0.64	0.24	0.53
Severn (Sampson et al. 2015)	0.83	0.23	0.67

559

560   The different masking applied to reference flood maps may explain some of the differences:

561   Sampson et al. removed all channels with upstream areas of less than 500 km^2, whereas here we

562   use a simpler 5 km buffer around modelled maps. The exclusion of permanent river channels in

563   our comparison may further penalize the overall score especially for the Thames, which as a rather

564   large channel estuary. Besides these differences in the validation, the better metrics of the maps

565   by Sampson et al. may depend on a more accurate hydrological input (based on regionalization

566   of gauge station data) and a better correction of urban elevation bias (based on a moving window

567   filter instead of the constant correction values applied here).

568   To provide further context, the US model by Wing et al. (2017) attained average CSI values of

569   ~0.75 against a number of detailed local models, whereas flood models built and calibrated for

570   local applications may achieve CSI scores up to 0.9 when benchmarked against very high quality

571   data (see Wing et al., 2019a). Fleischmann et al. (2019) recently proposed that regional-scale

572   models can provide locally relevant estimates of flood extent when CSI > 0.65. Although the

573   overall values shown in Table 3 are consistently below this threshold, better results are observed

574   for a number of river basins, as shown in Tables 4 and 5.

575

576

3.4 Comparison with the previous flood map dataset

577

578 Table 7 compares the performances of the flood hazard maps described in the present study
579 (version 2) with the previous version developed by Dottori et al. (2016a; version 1). The
580 comparison is shown for England and Hungary. Results for all other areas are comprised within
581 the range of results shown in Table 3. As can be seen, differences are generally reduced across
582 the different areas and return periods. Version 1 of the flood maps produced slightly better results
583 in Hungary for the 100- and 1000-year return period (increased CSI and HR, lower FAR), while
584 version 2 has somewhat improved performances in England, mainly driven by higher HR.

585

586 *Table 7. Comparison of performances of the flood hazard maps described in the present study*
587 *and developed by Dottori et al. (2016a). Table reports the ratio between flood extents (F2/F1)*
588 *and the difference between vVersion 2 and 1 of the HR, FAR and CSI values.*

589

	RP (years)	F2/F1	ΔHR	ΔFAR	ΔCSI
Hungary	30	0.97	-0.5%	-0.4%	2.9%
Hungary	100	1.00	-2.1%	0.7%	-2.4%
Hungary	1000	1.01	-3.6%	5.7%	-6.3%
England	100	1.05	9.4%	1.7%	7.3%
England	1000	1.04	8.2%	-1.1%	7.7%

590

591 These outcomes may be interpreted considering the changes in input data between the two
592 versions, and the structure of the modelling approach and of input data, which in turn has not
593 changed substantially. The main difference between the two map versions is given by the
594 hydrological input, with Version 2 using the latest calibrated version of the LISFLOOD model.
595 For the 100-year return period, peak flow values of Version 2 are on average 35% lower than
596 Version 1 in Hungary, and 16% lower in England. However, similar decreases are also observed
597 for the 1-in-2-year peak discharge that determines full-bank discharge. The resulting reduction in
598 channel hydraulic conveyance in respect to Version 1 is likely to offset the decrease of peak flood
599 volumes, which explain the small difference in overall flood extent given by the F2/F1 parameter
600 in Table 7. Such results confirm the low sensitivity of the modelling framework to the
601 hydrological input observed by Dottori et al. (2016) and by Trigg et al (2016) for a global-scale

602 application. It also confirms that the knowledge of river channel geometry is crucial to correctly
603 model the actual channel conveyance and thus improve inundation modelling. Other differences
604 in input data are given by minor changes in Manning's parameters and in the EFAS river network,
605 which might contribute to the observed differences.

606

607 *3.5 Influence of elevation data*

608 Table 8 compares the metrics calculated with CCM DEM elevation data against the same metrics
609 for the modelled flood maps based on MERIT-DEM. The comparison is carried out for England,
610 Hungary and the Po river basin. Performance is slightly improved by the use of MERIT-DEM
611 data for all areas and return periods, in particular through the reduction of FAR, even though the
612 overall increase of CSI values is limited to few percentage points.

613

614 *Table 8. Comparison of performances of the flood hazard maps described in the present study*
615 *and developed by Dottori et al. (2016a) based on the MERIT-DEM (a) and CCM-DEM (b). Table*
616 *reports the ratio between flood extents F and the differences for HR, FAR, and CSI (e.g. (HRa-*
617 *HRb)/HRa).*

618

	RP (years)	ΔF	ΔHR	ΔFAR	ΔCSI
Hungary	100	-5.3%	0.0%	-2.0%	5.1%
Hungary	1000	-5.9%	-0.1%	-7.6%	5.2%
England	100	0.0%	2.6%	-5.7%	3.8%
England	1000	1.7%	2.8%	-7.8%	3.2%
Po	500	0.2%	0.9%	-4.3%	3.4%

619

620 Because of this limited improvement and the considerable amount of time required to re-run the
621 complete set of flood hazard maps (several days for each return period) it was decided not to
622 update the flood maps using the MERIT-DEM as elevation data. Moreover, new high-resolution
623 datasets such as the Copernicus DEM (ESA-Airbus 2019), the 90m version of TanDEM-X dataset
624 (https://geoservice.dlr.de/web/dataguide/tdm90), and MERIT-HYDRO (Yamazaki et al., 2019)
625 have recently become available, and therefore future research could focus on performing

626   additional comparisons to identify which dataset is most suitable for inundation modelling in
627   Europe.
628

4) Conclusions and ongoing work

630   We presented here a new dataset of flood hazard maps covering the geographical Europe and
631   including large parts of the Middle East and river basins entering the Mediterranean Sea. This
632   dataset significantly expands the previous available flood maps datasets at continental scale
633   (Alfieri et al., 2014; Dottori et al., 2016a), and therefore constitutes a valuable source of
634   information for future research studies and flood management, especially for countries where no
635   official flood hazard maps are available. The new maps also benefit of updated models and new
636   calibration and meteorological data. The maps are being used for a range of applications at
637   continental scale, from evaluating present and future river flood risk scenarios, to the cost-benefit
638   assessment of different adaptation strategies to reduce flood impacts, and for comparisons
639   between different regions, countries and river basins (Dottori et al, 2020b). Moreover, the flood
640   hazard maps are designed to be integrated with the Copernicus European Flood Awareness
641   System (EFAS), and will be used to perform operational flood impact forecasting in EFAS
642   (Dottori et al., 2017).
643   We performed a detailed validation of the modelled flood maps in several European countries
644   against official flood hazard maps. The resulting validation exercise is the most complete
645   undertaken so far for Europe to our best knowledge, and provided a comprehensive overview of
646   the strengths and limitations of the new maps. Nevertheless, the unavailability of reference flood
647   maps outside Europe did not allow any validation in the arid regions in North Africa and Eastern
648   Mediterranean. In these areas, further research will be needed to better understand the
649   performance of the flood mapping procedure here proposed. Modelled maps generally achieve
650   low scores for high and medium probability of flooding. For the 1-in-100-year return period, the
651   modelled maps can identify on average two-thirds of reference flood extent, however they also
652   largely overestimate flood-prone areas in many regions, thus hampering the overall performance.
653   Performances improves markedly with the increasing of return period, mostly due to the decrease
654   of the false alarm rates. In particular, critical success index (CSI) values approach and in some
655   cases exceed 0.5 for return periods equal or above 500 years, meaning that the maps can correctly

656 identify more than half of flooded areas in the main river stems and tributaries of different river
657 basins.

658 It is important to note that the validation was affected by problems in identifying the correct areas
659 for a fair comparison, because of the different density of the mapped river network in reference
660 and modelled maps. In our study we used large buffers to constrain comparison areas, which
661 possibly penalized the model performance by generating spurious false alarms in areas not
662 considered by official maps. However, we observed that the proposed maps achieve comparable
663 results to other large-scale flood models when using similar parameters for the validation.

664 The low skill of modelled maps for high and medium probability of flooding, with large
665 overestimations observed in different lowland areas, is likely motivated by the non-inclusion of
666 flood defences in the modelling framework and the simplified representation of channel hydraulic
667 conveyance, due to the absence of datasets at European scale describing river channels and
668 defence structures (i.e. design standards and location of dyke systems). Such information
669 combined with high-resolution DEM fed with local-scale information (artificial and defence
670 structures) is crucial to improve the performance of large-scale flood models and apply more
671 realistic flood modelling tools, as observed also by Wing et al (2017, 2019b). Uncertainty in peak
672 flow estimation can also influence the skill of the modelled maps; however, we found that the
673 limited sensitivity of the modelling approach to changes in the hydrological input smooths out
674 this uncertainty source, because channel conveyance is linked to streamflow characteristics. Such
675 finding highlight the need for independent data of river channel width, shape and depth to better
676 reproduce streamflow and flooding processes. Moreover, the improved results offered by the use
677 of the MERIT-DEM elevation data suggest that recent high-resolution datasets such as the
678 Copernicus DEM (ESA-Airbus 2019), TanDEM-X
679 (https://geoservice.dlr.de/web/dataguide/tdm90), and MERIT-HYDRO (Yamazaki et al., 2019)
680 may offer a viable solution to improve future versions of continental-scale flood hazard maps in
681 Europe.

682 Increasing map coverage by including the minor river network is likely to improve the skill of
683 modelled maps. However, this might require the use of a different modelling approach to account
684 for pluvial flooding (Wing et al., 2017; Bates et al., 2021), along with reliable model climatology
685 to represent small-scale precipitation processes. Improving the simulation of reservoirs may also

686 reduce the difference between the real and modelled hydrological regimes in regions such as the
687 Iberian Peninsula and the Alps.

Data availability

689 The dataset described in this manuscript is accessible as part of the data collection "Flood Hazard
690 Maps at European and Global Scale" at the JRC Data Catalogue
691 (https://data.jrc.ec.europa.eu/collection/floods/).

692 Please refer to the dataset as follows: Dottori F., Bianchi A., Alfieri, L., Skoien, J., Salamon P.,
693 2020. River flood hazard maps for Europe and the Mediterranean Basin ~~region~~. JRC Data
694 Catalogue, accessibile at http://data.europa.eu/89h/1d128b6c-a4ee-4858-9e34-6210707f3c81 .
695 doi: 10.2905/1D128B6C-A4EE-4858-9E34-6210707F3C81

696 Note that the DOI for the dataset will be available soon. The dataset comprises the following
697 maps (eight in total), each one available as a raster (Geotiff) file:

698 • Map of permanent water bodies for Europe and the Mediterranean Basin ~~region~~
699 • River network in Europe and the Mediterranean Basin ~~region~~
700 • River flood hazard maps for Europe and the Mediterranean Basin ~~region~~ (return periods of
701 10, 20, 50, 100, 200 and 500 years)

702 The official flood hazard maps used for the validation exercise are freely accessible at the
703 following web-sites:

704 • Spain: https://www.miteco.gob.es/es/cartografia-y-sig/ide/descargas/agua/zi-lamina.aspx (in
705 Spanish)
706 • Po River Basin: https://pianoalluvioni.adbpo.it/progetto-esecutivo-delle-attivita/ (in Italian)
707 • Norway: https://www.nve.no/flaum-og-skred/kartlegging/flaum/ (in Norwegian)
708 • England: https://data.gov.uk/dataset/bed63fc1-dd26-4685-b143-2941088923b3/flood-map-
709 for-planning-rivers-and-sea-flood-zone-3 ; https://data.gov.uk/dataset/cf494c44-05cd-4060-
710 a029-35937970c9c6/flood-map-for-planning-rivers-and-sea-flood-zone-2 (in English)
711 • Hungary: https://www.vizugy.hu/index.php?module=content&programelemid=62 (in
712 Hungarian)

713 The LISFLOOD hydrological model used in this research is released as open-source software and
714 available at https://ec-jrc.github.io/lisflood/.

715 The streamflow dataset derived from the long-term run of the LISFLOOD model is available at
716 https://cds.climate.copernicus.eu/cdsapp#!/dataset/efas-historical
717 The LISFLOOD-FP hydrodynamic model used in this research is available as open-source
718 software at https://www.seamlesswave.com/LISFLOOD8.0 for research and non-commercial
719 purposes.
720

Appendix A: Meteorological observations used for LISFLOOD simulations

722 The long-term run of the hydrological model LISFLOOD is based on observed data from
723 meteorological stations and precipitation datasets, which are collected and continuously expanded
724 as part of the development work for EFAS. The meteorological variables considered are:
725 precipitation, minimum and maximum temperature, wind speed, solar radiation and vapour
726 pressure. The number of stations with available meteorological observations depends on the
727 period and variable considered, with an increasing availability towards the end of the historical
728 simulation period. As an example, for the year 2016 the number of daily observations available
729 ranged from ~8.800 for temperature to ~5.500 for precipitation and ~3.700 for vapour pressure.
730 The input from meteorological stations is completed by a number of precipitation datasets
731 (EURO4M-APG, INCA-Analysis Austria, ERA-Interim GPCP corrected and Carpat-Clim; for
732 details see Arnal et al., 2019). Note that the same datasets are used to drive the LISFLOOD
733 calibration and to calculate the initial conditions for the EFAS forecasts. The data from
734 meteorological stations and gridded datasets were then interpolated using the interpolation
735 scheme SPHEREMAP to produce meteorological grids with a daily time step. The reader is
736 referred to Arnal et al. (2019) for further details.
737

Appendix B: LISFLOOD calibration and validation results

739 We report here an overview of the results of the LISFLOOD calibration and validation presented
740 by Arnal et al. (2019). The skill of LISFLOOD in reproducing observed flow regimes
741 (hydrological skill) is expressed using two indices, the Kling-Gupta Efficiency (KGE; Gupta et
742 al., 2009) and the Nash-Sutcliffe Efficiency (NSE; Nash and Sutcliffe, 1970). The NSE index is
743 widely applied in literature and is useful to measure the hydrological skill under high-flow

744 conditions, given its sensitivity to flow extremes (Krause et al., 2005). The KGE index provides
745 a more complete evaluation of the model skill under variable flow conditions, and is therefore
746 useful for calibration purposes (Gupta et al., 2009; Knoben et al., 2019)
747 Table B1 summarizes the results of KGE and NSE indices, and Figure B1 shows the spatial
748 distribution of the KGE index values across the EFAS domain. The spatial distribution of NSE is
749 roughly similar. For a detailed list of scores for all stations, please refer to Arnal et al. (2019).
750
751 *Table B1. Overview of the hydrological skill of LISFLOOD for the calibration and validation*
752 *stations.*

	calibration		validation			calibration		validation	
NSE	**no. of stations**	**[%]**	**no. of stations**	**[%]**	**KGE**	**no. of stations**	**[%]**	**no. of stations**	**[%]**
> 0.75	147	21%	101	14%	**> 0.75**	303	42%	174	24%
> 0.5–0.75	277	39%	207	30%	**> 0.5–0.75**	240	33%	235	33%
> 0.2–0.5	165	23%	171	25%	**> 0.2–0.5**	91	13%	172	24%
> 0–0.2	35	5%	65	9%	**> 0–0.2**	36	5%	44	6%
≤0	93	13%	153	22%	**≤0**	47	7%	73	10%
	∑ **717**		∑ **698**			∑ **717**		∑ **698**	

753
754 As can be seen from Table B1, 75 % of all stations scored a KGE higher than 0.5 during
755 calibration, and 57 % during validation. NSE index values above 0.5 are scored for 60% and 44%
756 of stations, respectively for the calibration and validation periods.
757 It is clearly noticeable that the skill is not homogeneously distributed across Europe, with higher
758 skills in large parts of Central Europe, and lower skill mostly in Spain caused by the strong
759 influence of reservoirs and flow control structures. The other study areas considered in the
760 validation exercise (England, Hungary, Norway, Po river basin) exhibit KGE and NSE values
761 generally above 0.5.
762

763
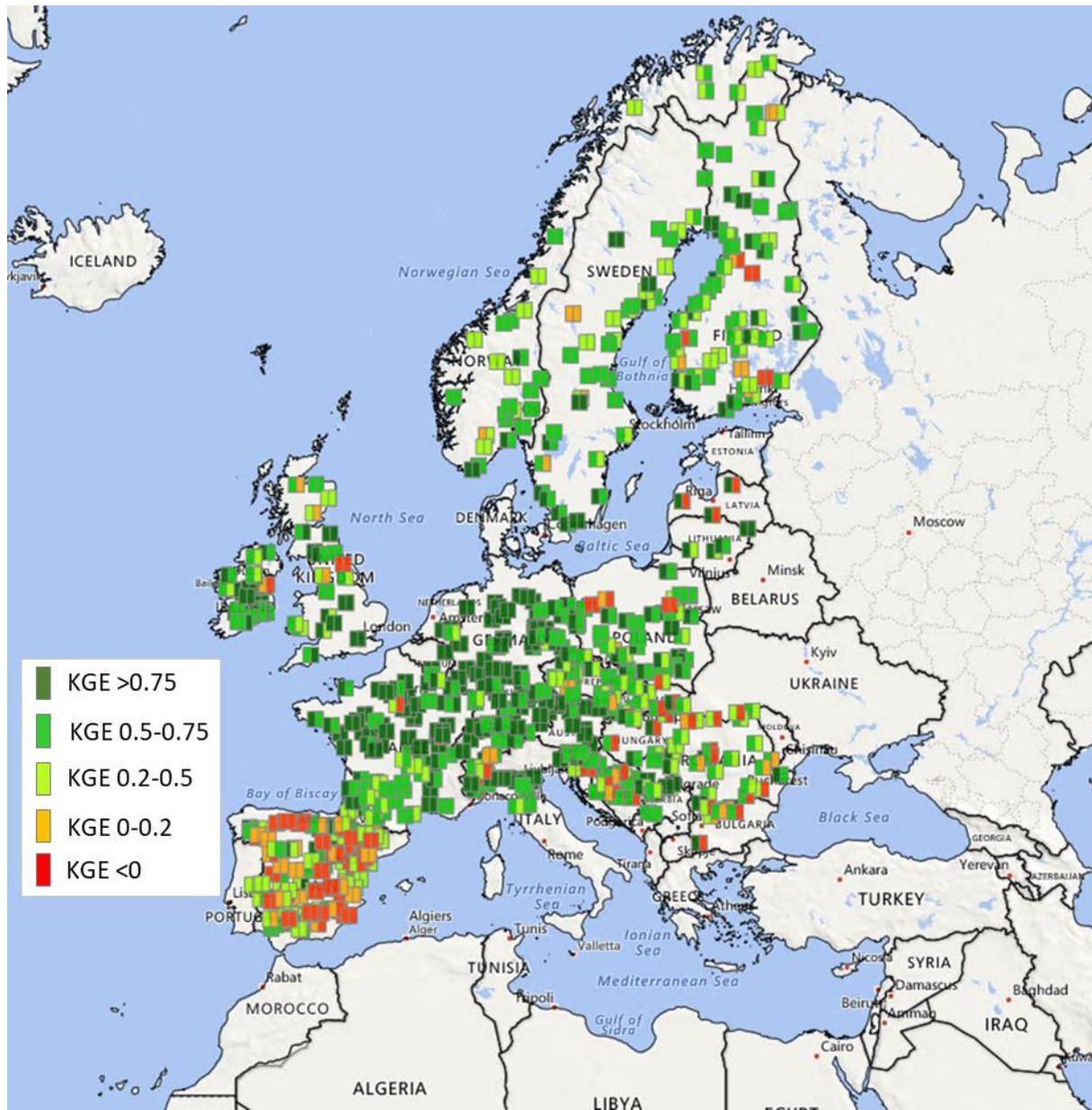
Figure B1. Hydrological skill of EFAS at the calibration locations. Colour coding denotes the
quality of the KGE during calibration (left half of square) and validation (right half of the square).
Adapted from Arnal et al. (2019).

767

768

Appendix C: Additional results

C1: validation results for the Po River Basin

According to Table 3, the modelled flood maps provide a better reproduction of reference maps for the Po River, compared to other study areas. False alarms are low, while hit ratio (HR) values indicate that two out of every three pixels in the reference map are correctly identified as flooded. The analysis of reference and modelled maps (Figure C1), suggests that the underestimation is partly caused by flooded areas along some tributaries which are not included in modelled maps. Other areas with omission errors are located near confluences of the Po main stem and the major tributaries in Emilia-Romagna, which may depend on the underestimation of peak flow on tributaries. In fact, the results of the LISFLOOD calibration in Figure B1 show better hydrological skill along the Po main stem, compared to some tributaries. Finally, it is likely that the inclusion of smaller tributaries of the river network in the modelled maps would improve the overall performance.
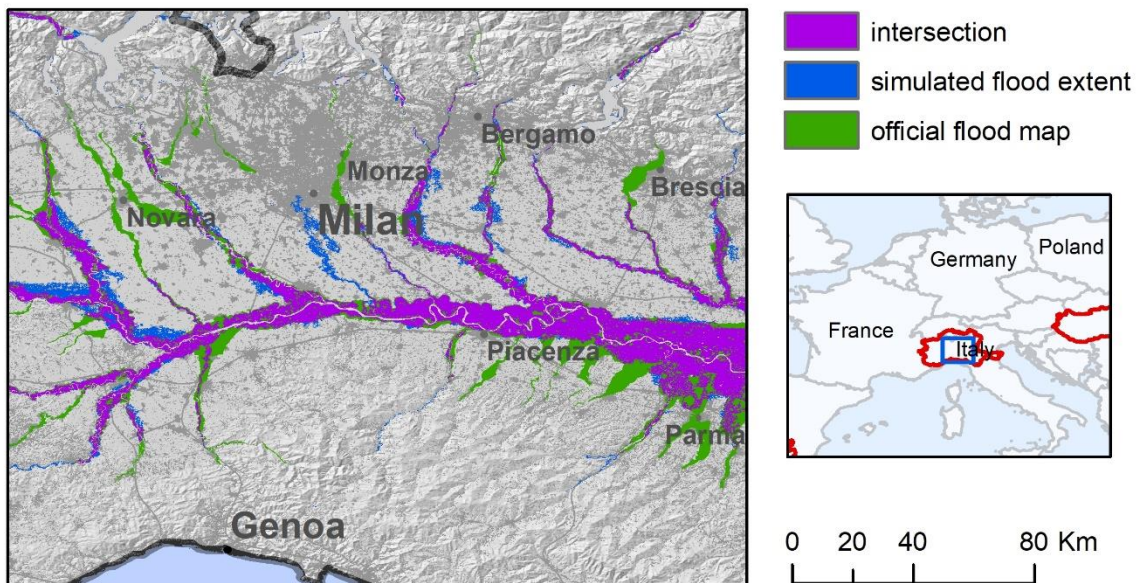
Figure C1. Comparison of modelled (blue) and reference (green) flood hazard maps (1-in-500-year) over the Po river basin, Italy. Purple areas denotes the intersection (agreement) between the two set of maps.

C2: validation results for Norway

788

789 The results of the modelled flood maps in Norway show a general tendency to overestimate flood
790 extent for the 1-in-100-year events, with high values for both hit ratio (HR) and false alarm ratio
791 (FAR). Such a result is in fact largely influenced by the relatively small extent and discontinuous
792 coverage of reference maps. Flood-prone areas for the 1-in-100-year official maps only cover 215
793 km^2, possibly due to the low density of populated places in Norway, while they cover between
794 4700 and 5700 km^2 for England, Spain and Hungary. As for Spain, we applied a 5km buffer to
795 restrict the area of comparison around reference maps, yet this leads to spurious overestimation
796 around the edges of reference map polygons. Notably, the performance improves markedly with
797 the use of a 1km buffer as in Wing et al., (2017), which results in increased critical success index
798 (CSI) scores up to nearly 0.50.
799 The results of reported by Arnal et al. (2019) and summarized in Figure B1 suggest an acceptable
800 hydrological skill of the LISFLOOD calibration in Norway, with a majority of gauge stations
801 scoring KGE values above 0.5. In the areas with lower scores, the model performance for low-
802 probability flood events might be influenced by an incorrect estimation of peak discharges driven
803 by snow melt, which plays a relevant role in determining low-probability flood events.

804

C3: Influence of correcting elevation data with land use

805

806 We tested the results of correcting CCM DEM elevation data with vegetation cover in
807 Scandinavia, where the percentage of land covered by forests is more relevant than in the other
808 regions included in the modelled flood maps. For the 1-in100-year flood maps, the overall
809 difference in flood extent between the corrected and uncorrected maps is less than 4%, and similar
810 values were found for the other return periods. Moreover, the HR, FAR and CSI values   of two
811 set of maps differ by less that 2% when calculated against the 1-in100-year official map in
812 Norway, probably because forested areas have not been considered as relevant flood-prone areas.
813 These results suggest that the simulation of densely vegetated areas have a limited importance in
814 determining the overall performance of modelled flood maps in Europe.

815

816

Author contribution

817

818

819 FD: conceptualization, formal analysis, investigation, data curation writing (original draft, review
820 and editing); LA: methodology, investigation, writing (review and editing); AB: data curation,
821 validation, visualization; JS: investigation, writing (review and editing); PS: conceptualization,
822 project administration, writing (original draft, review and editing)

823

Competing interests

824

825 The authors declare that they have no conflict of interest.

826

Acknowledgements

827

828 This study has been partially funded by the COPERNICUS programme and by an administrative
829 arrangement with Directorate General 'European Civil Protection and Humanitarian Aid
830 Operations (DG ECHO) of the European Commission. EFAS is operated and financed as part of
831 the Copernicus Emergency Management Service. The authors would like to thank Niall
832 McCormick for his valuable suggestions on the early versions of the manuscript

833

834

References

Alfieri, L., Salamon, P., Bianchi, A., Neal, J., Bates, P.D., Feyen, L., 2014. Advances in pan-European flood hazard mapping, Hydrol. Process.,28 (18), 4928-4937, doi:10.1002/hyp.9947.

Alfieri L., Feyen L., Dottori F., Bianchi A., 2015. Ensemble flood risk assessment in Europe under high end climate scenarios. Global Environmental Change 35, 199–212.

Alfieri, L., L. Feyen, and G. D. Baldassarre (2016), Increasing flood risk under climate change: a pan-European assessment of the benefits of four adaptation strategies, Clim. Change, 136(3), 507–521, doi:10.1007/s10584-016-1641-1.

Arnal, L., S.-S. Asp, C. Baugh, A. de Roo, J. Disperati, F. Dottori, R. Garcia, M. GarciaPadilla, E. Gelati, G. Gomes, M. Kalas, B. Krzeminski, M. Latini, V. Lorini, C. Mazzetti, M. Mikulickova, D. Muraro, C. Prudhomme, A. Rauthe-Schöch, K. Rehfeldt, P. Salamon, C. Schweim, J.O. Skoien, P. Smith, E. Sprokkereef, V. Thiemig, F. Wetterhall, M. Ziese, 2019. EFAS upgrade for the extended model domain – technical documentation, EUR 29323 EN, Publications Office of the European Union, Luxembourg, 2019, ISBN 978-92- 79-92881-9, doi: 10.2760/806324, JRC111610.

Autorita` di bacino del fiume Po (AdB Po): Progetto di Variante al PAI: mappe della pericolosita` e del rischio di alluvione (in Italian), https://pianoalluvioni.adbpo.it/progetto-esecutivodelleattivita/, accessed on 2020-04-03, 2012.

Bates, P. D., De Roo, A. P. J., 2000. A simple raster-based model for flood inundation simulation, J. Hydrol., 236 (1–2), 54–77.

Bates P.D., Horritt M.S., and Fewtrell T.J., 2010. A simple inertial formulation of the shallow water equations for efficient two-dimensional flood inundation modelling. Journal of Hydrology, 387, 33-45.

Bates, P. D., Quinn, N., Sampson, C., Smith, A., Wing, O., Sosa, J., et al. (2021). Combined modeling of US fluvial, pluvial, and coastal flood hazard under current and future climates. Water Resources Research, 57, e2020WR028673. https://doi.org/10.1029/2020WR028673

Baugh, C. A., Bates, P. D., Schumann G., Trigg, M.A., 2013. SRTM vegetation removal and hydrodynamic modeling accuracy, Water Resour. Res. 49, 5276–5289, doi:10.1002/wrcr.20412.

Barredo JI, de Roo A, Lavalle C. 2007. Flood risk mapping at European scale. Water Science and Technology 56: 11–17.

865   Bontemps, S., et al., 2009. GLOBCOVER -Products description and validation report, Univ.
866 Catholique de Louvain.

867   Burek, P., Knijff van der, J., Roo de, A., 2013. LISFLOOD, Distributed Water Balance and
868 Flood Simulation Model Revised User Manual 2013. Publications Office, Luxembourg.

869   Copernicus Land Monitoring Service. Corine Land Cover. http://land.copernicus.eu/pan-
870 european/corine-land-cover (accessed on 12/2/2020).

871   Dottori, F., Alfieri, L., Salamon, P., Bianchi, A., Feyen, L., Lorini, V., 2016a: Flood hazard
872 map for Europe - 100-year return period. European Commission, Joint Research Centre (JRC)
873 [Dataset] PID: http://data.europa.eu/89h/jrc-floods-floodmapeu_rp100y-tif

874   Dottori, F., Salamon, P., Bianchi, A., Alfieri, L., Hirpa, F.A., Feyen, L., 2016b. Development
875 and evaluation of a framework for global flood hazard mapping. Advances in Water Resources
876 94, 87–102.

877   Dottori F., Kalas M.,Salamon P., Bianchi A., Alfieri, L., Feyen L., 2017. An operational
878 procedure for rapid flood risk assessment in Europe. Nat. Hazards Earth Syst. Sci., 17, 1111-
879 1126, https://doi.org/10.5194/nhess-17-1111-2017.

880   Dottori, F., Szewczyk, W., Ciscar, J.C., Zhao, F., Alfieri, L., Hirabayashi, Y., Bianchi, A.,
881 Frieler, K., Betts, R.A., Feyen, L., 2018 Increased human and economic losses from river floods
882 with anthropogenic warming. Nature Climate Change, 8(9), 781-786,
883 https://doi.org/10.1038/s41558-018-0257-z

884   Dottori F., Bianchi A., Alfieri, L., Skoien, J., Salamon P., 2020a. River flood hazard maps for
885 Europe and the Mediterranean Basin region. JRC Data Catalogue, accessibile at
886 https://data.jrc.ec.europa.eu/dataset/1d128b6c-a4ee-4858-9e34-6210707f3c81 .

887   Dottori F, Mentaschi L, Bianchi A, Alfieri L and Feyen L, 2020b. Adapting to rising river
888 flood risk in the EU under climate change, EUR 29955 EN, Publications Office of the European
889 Union, Luxembourg, 2020, ISBN 978-92-76-12946-2 , doi:10.2760/14505, JRC118425.

890   European Commission (EC), 2007. Directive 2007/60/EC of the European Parliament
891 and of the Council on the assessment and management of flood risks, Official Journal
892 of the European Communities, Brussels, available at: http://eur-lex.europa.eu/legal-
893 content/EN/TXT/?uri=CELEX%3A32007L0060 (accessed on 13/5/2020).

ESA-Airbus, 2019. Copernicus Digital Elevation Model Validation Report, accessed on 14/5/2020 at https://spacedata.copernicus.eu/documents/12833/20611/GEO1988-CopernicusDEM-RP-001_ValidationReport_V1.0/9bc5d392-c5f2-4118-bd60-db9a6ea4a587

Feyen L, Dankers R, Bódis K, Salamon P, Barredo JI. 2012. Fluvial floodrisk in Europe in present and future climates. Climatic Change: 112(1): 47–62, doi:10.1007/s10584-011-0339-7.

Fleischmann A., R. Paiva, W. Collischonn, 2019. Can regional to continental river hydrodynamic models be locally relevant? A cross-scale comparison. Journal of Hydrology X, 2019.

Gupta, H.V., H. Kling, K.K. Yilmaz, G.F. Martinez, 2009: Decomposition of the mean squared error and NSE performance criteria: implications for improving hydrological modelling. Journal of Hydrology, 377, 80-91.

Hirpa, F.A.; Salamon, P.; Beck, H.E.; Lorini, V.; Alfieri, L.; Zsoter, E.; Dadson, S.J. , 2018. Calibration of the Global Flood Awareness System (GloFAS) using daily streamflow data. J. Hydrol., 566, 595–606.

Jongman, B., Hochrainer-Stigler, S., Feyen, L., Aerts, J.C.J.H., Mechler, R., Botzen, W.J.W., Bouwer, L.M., Pflug, G., Rojas, R., Ward, P.J., 2014. Increasing stress on disaster-risk finance due to large floods. Nat. Clim. Change 4, 264-268, doi:http://dx.doi.org/10.1038/nclimate2124.

Knoben, W. J. M., Freer, J. E., and Woods, R. A.: Technical note: Inherent benchmark or not? Comparing Nash–Sutcliffe and Kling–Gupta efficiency scores, Hydrol. Earth Syst. Sci., 23, 4323–4331, https://doi.org/10.5194/hess-23-4323-2019, 2019.

Krause, P., Boyle, D. P., Bäse, F. Comparison of different efficiency criteria for hydrological model assessment. Advances in Geosciences, European Geosciences Union, 2005, 5, pp.89-97.

Kulp, S.A.; Strauss, B.H. CoastalDEM: A global coastal digital elevation model improved from SRTM using a neural network. Remote Sens. Environ. 2018, 206, 231–239.

Liu, Y., Bates, P.D., Neal, J.C. and Yamazaki, D., 2019, December. Bare-earth DEM Generation in Urban Areas Based on a Machine Learning Method. In AGU Fall Meeting Abstracts (Vol. 2019, pp. H41N-1899).

Meadows, M.;Wilson, M. A Comparison of Machine Learning Approaches to Improve Free Topography Data for Flood Modelling. Remote Sens. 2021, 13, 275. https://doi.org/10.3390/rs13020275

Ministerio de Medio Ambiente y Medio Rural y Marino (MITECO), 2011. Guía Metodologica para el desarrollo del sistema nacional de cartografia de zonas inundables. Accessed on 18/5/2020 at https://www.miteco.gob.es/es/agua/temas/gestion-de-los-riesgos-de-inundacion/snczi/Guia-metodologica-determinacion-zonas-inundables/default.aspx (in Spanish).

Nash, J. E. and Sutcliffe, J. V.: River flow forecasting through conceptual models part I – A discussion of principles, J. Hydrol., 10, 282–290, https://doi.org/10.1016/0022-1694(70)90255-6, 1970.

The Norwegian Water Resources and Energy Directorate, 2020. Flood Zone Maps. Accessed on 24/4/2020 at https://www.nve.no/flaum-og-skred/kartlegging/flaum/ (in Norwegian)

Paprotny, D., Morales-Nápoles, O., and Jonkman, S. N.: Efficient pan-European river flood hazard modelling through a combination of statistical and physical models, Nat. Hazards Earth Syst. Sci., 17, 1267-1283, https://doi.org/10.5194/nhess-17-1267-2017, 2017.

Sampson, C. C., Smith, A. M., Bates, P. D., Neal, J. C., Alfieri, L., & Freer, J. E. (2015). A high-resolution global flood hazard model. *Water Resources Research*, *51*(9), 7358-7381.

Scussolini, P., Aerts, J. C. J. H., Jongman, B., Bouwer L. M., Winsemius H. C., de Moel H., and Ward, P. J., 2015. FLOPROS: an evolving global database of flood protection standards. Nat. Hazards Earth Syst. Sci. Discuss., 3, 7275–7309, 2015, doi:10.5194/nhessd-3-7275-2015.

Shaw, J., Kesserwani, G., Neal, J., Bates, P., and Sharifian, M. K.: LISFLOOD-FP 8.0: the new discontinuous Galerkin shallow-water solver for multi-core CPUs and GPUs, Geosci. Model Dev., 14, 3577–3602, https://doi.org/10.5194/gmd-14-3577-2021, 2021.

Thielen J., Bartholmes J., Ramos M.H., and De Roo A. (2009). The European flood alert system - part 1: concept and development. Hydrol. Earth Syst. Sci. 13, 125-140.

Trigg, M. et al., 2016. The credibility challenge for global fluvial flood risk analysis. Environ. Res. Lett.11 094014

United Nations Office for Disaster Risk Reduction (UNISDR), 2015. Sendai Framework for Disaster Risk Reduction 2015–2030 (www.unisdr.org/we/inform/publications/43291)

Van der Knijff, J.M., Younis, J., de Roo, A.P.J., 2010. LISFLOOD: a GIS-based distributedmodel for river basin scale water balance and flood simulation. Int. J. Geogr. Inf. Sci. 24, 189-212.

Vogt et al., 2007. A pan-European river and catchment database, JRC Reference Reports, doi:0.2788/35907.

Ward, P.J. et al., 2015. Usefulness and limitations of global flood risk models. Nature Climate Change 5, 712–715.

Wendi, D.; Liong, S.-Y.; Sun, Y.; Doan, C.D. An innovative approach to improve SRTM DEM using multispectral imagery and artificial neural network. J. Adv. Model. Earth Syst. 2016, 8, 691–702.

Wing, O. E., Bates, P. D., Sampson, C. C., Smith, A. M., Johnson, K. A., & Erickson, T. A. (2017). Validation of a 30 m resolution flood hazard model of the conterminous United States. Water Resources Research, 53(9), 7968-7986, doi:10.1002/2017WR020917.

Wing, O. E. J., Sampson, C. Bates, P. D., Quinn, N., Smith, A. M., Neal, J. C., C. (2019a). A flood inundation forecast of Hurricane Harvey using a continental-scale 2D hydrodynamic model. Journal of Hydrology X 4 , 100039.

Wing, O. E. J., Bates, P. D., Neal, J. C., Sampson, C. C., Smith, A. M., Quinn, N., et al. (2019b). A New Automated Method for Improved Flood Defense Representation in Large-Scale Hydraulic Models. Water Resources Research 55, 11007-11034, https://doi.org/2019WR025957

Yamazaki, D., Ikeshima, D., Tawatari, R., Yamaguchi, T., O'Loughlin, F., Neal, J., Sampson, C., Kanae, S., Bates, P. D. (2017). A high accuracy map of global terrain elevations. Geophysical Research Letters.

Yamazaki, D., Ikeshima, D., Sosa, J., Bates, P. D., Allen, G. H., & Pavelsky, T. M. (2019). MERIT Hydro: a high-resolution global hydrography map based on latest topography dataset. Water Resources Research, 55, 5053–5073. https://doi.org/10.1029/2019WR024873

Zuzanna Zajac, Z:, Zambrano-Bigiarini, M., Salamon, P., Burek, P., Gentile, A., Bianchi, A., 2013. Calibration of the LISFLOOD hydrological model for Europe. JRC technical report JRC87717.